(6) Glandt, E. D. *J. Colloid Interface Sci.* **1980**, *77*, 512.
(7) Anderson, J. L.; Brannon, J. H. *J. Polym. Sci., Polym. Phys. Ed.* **1981**, *19*, 405.
(8) Mitchell, B. D.; Deen, W. M. *J. Membr. Sci.* **1984**, *19*, 75.
(9) Fanti, L. A.; Glandt, E. D. *J. Colloid Interface Sci.* **1990**, *135*, 385, 396.
(10) Casassa, E. F. *J. Polym. Sci., Polym. Lett. Ed.* **1967**, *5*, 773.
(11) Casassa, E. F.; Tagami, Y. *Macromolecules* **1969**, *2*, 14.
(12) Davidson, M. G.; Suter, U. W.; Deen, W. M. *Macromolecules* **1987**, *20*, 1141.
(13) Davidson, M. G.; Deen, W. M. *J. Polym. Sci., Polym. Phys. Ed.* In press.
(14) Zhulina, E. B.; Gorbunov, A. A.; Birshtein, T. M.; Skvortsov, A. M. *Biopolymers* **1982**, *21*, 1021.
(15) Gorbunov, A. A.; Zhulina, E. B.; Skvortsov, A. M. *Polymer* **1982**, *23*, 1133.
(16) Pouchlý, J. *J. Chem. Phys.* **1970**, *52*, 2567.
(17) de Gennes, P.-G. *Rep. Prog. Phys.* **1969**, *32*, 187.
(18) Yamakawa, H. *Modern Theory of Polymer Solutions*; Harper and Row: New York, 1971; pp 110–118.
(19) Jones, I. S.; Richmond, P. *J. Chem. Soc., Faraday Trans. 2* **1977**, *73*, 1062.
(20) Lepine, Y.; Caille, A. *Can. J. Phys.* **1978**, *56*, 403.
(21) Wiegel, F. W. *J. Phys. A* **1977**, *10*, 299.
(22) Flory, P. J. *Principles of Polymer Chemistry*; Cornell University Press: Ithaca, NY, 1953.
(23) de Gennes, P.-G. *Scaling Concepts in Polymer Physics*; Cornell University Press: Ithaca, NY, 1979; pp 246–248.
(24) DiMarzio, E. A. *J. Chem. Phys.* **1965**, *42*, 2101.
(25) Press, W. H.; Flannery, B. P.; Teukolsky, S. A.; Vetterling, W. T. *Numerical Recipes*; Cambridge University Press: Cambridge, 1986; pp 637–638.
(26) Deen, W. M. *AIChE J.* **1987**, *33*, 1409.
(27) Israelachvili, J. N. *Intermolecular and Surface Forces*; Academic Press: London, 1985.
(28) Reiss, H. *J. Chem. Phys.* **1967**, *47*, 186.
(29) Bailey, J. M. *Macromolecules* **1977**, *10*, 725.
(30) Derby, J. J.; Atherton, L. J.; Thomas, P. J.; Brown, R. A. *J. Scientific Comput.* **1987**, *2*, 297.
(31) Glass, L. In *Modern Theoretical Chemistry. Vol. 6. Statistical Mechanics, Part B. Time Dependent Processes*; Berne, B. J., Ed.; Plenum: New York, 1977, pp 29–32.
(32) Acton, F. S. *Numerical Methods That Work*; Harper and Row: New York, 1970; pp 331–334.
(33) Amundson, N. R. *Mathematical Methods in Chemical Engineering*; Prentice-Hall: Englewood Cliffs, NJ, 1974; pp 143–147.

Mutual Diffusion of Block Polymer and Homopolymer. Visualization Using Microdomain as a Probe

Satoshi Koizumi, Hirokazu Hasegawa, and Takeji Hashimoto*

Department of Polymer Chemistry, Faculty of Engineering, Kyoto University, Kyoto 606, Japan

Received October 2, 1989; Revised Manuscript Received November 30, 1989

ABSTRACT: Poly(styrene-*b*-isoprene) block polymer (SI), which forms spherical microdomains of polyisoprene (PI) block chains in the matrix of polystyrene (PS) block chains, and a mixture of SI with homopolystyrene (HS), which forms spherical microdomains of PI in the matrix of HS and PS block chains, were welded with HS with a molecular weight smaller than that of PS. The welded samples were annealed at 150 °C as a function of time, and a spatial distribution of PI spherical microdomains across the welded interface $\phi(x)$ (x being a distance normal to the interface) was observed under a transmission electron microscope in order to investigate mutual diffusion of HS molecules and PI spherical microdomains with PS chains emanating from them. The mutual diffusion coefficient, D, was found to increase with increasing the volume fraction of HS (Ψ_{HS}) initially solubilized into the microdomain space and with decreasing the molecular weight of HS (M_{HS}). D was found to be controlled primarily by the free energy barrier $\delta\Delta F^*(\Psi_{HS}, M_{HS})$ required for solubilization of HS into the matrix of the microdomain systems in the mutual diffusion process. The free energy barrier for the mutual diffusion process, $\delta\Delta F^*$, in turn, is associated with a loss of conformational entropy of the HS and PS block chains in the solubilization process, which involves breakup of the molecular interactions of PS block chains. More precisely, we found that the diffusion process does not generally obey a simple Fickian diffusion; the concentration profile $\phi(x)$ is asymmetric, and D depends on the local concentration of HS ($\phi_{HS}(x)$), that is, the larger the $\phi_{HS}(x)$, the larger the value $D(x)$, and hence on space x.

I. Introduction

Mutual diffusion of polymers in bulk is an interesting research topic in polymer physics.[1-4] Here we propose visual observations of the mutual diffusion process of a unique polymer system. We study a mutual diffusion of a block polymer and a homopolymer, which are welded together at their fractured surfaces.

The block polymer system we used in this study is poly(styrene-*b*-isoprene) (SI) which forms spherical microdomains of polyisoprene block chains (PI) in the matrix of polystyrene block chains (PS) as shown schematically in Figure 1a. We used also a mixture of SI and homopolystyrene (HS), which forms PI spherical microdomains in the matrix of PS and HS as shown schematically in Figure 1b. HS was more or less uniformly solubilized into PS matrix formed by segregation of the block polymer.

SI block polymer in bulk or the bulk of the block polymer containing HS is welded with bulk HS at their surfaces, as shown schematically in Figure 2. The welded samples are then annealed at temperatures above glass transition temperatures of PS and HS to allow the mutual diffusion of HS chains and PI spheres across the welded interface. PI spheres have many PS chains emanating from them ("PS coronas"). The mutual diffusion will cause a change of spatial distribution of PI spheres across the interface as schematically sketched in parts a and b of

0024-9297/90/2223-2955$02.50/0

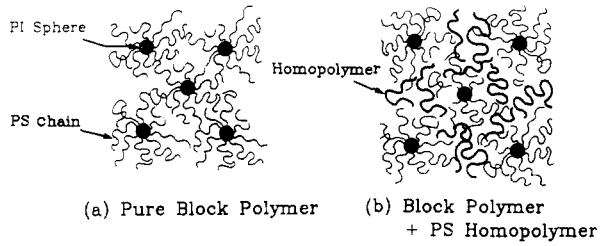

Figure 1. Schematic illustrations of the polymer systems used in this study: (a) pure SI block polymer system composed of the PI spherical microdomains forming a BCC lattice and PS matrix and (b) a mixture of the SI block polymer and homopolystyrene composed of PI spherical microdomains forming a BCC lattice and matrix of PS block chains and homopolystyrene.

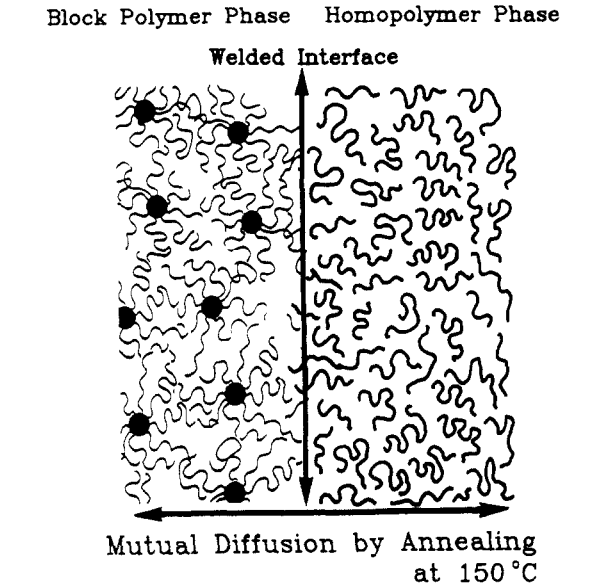

Figure 2. Schematic illustration of the cross section of the welded interface of an SI diblock polymer (left) and homopolystyrene (right) before annealing.

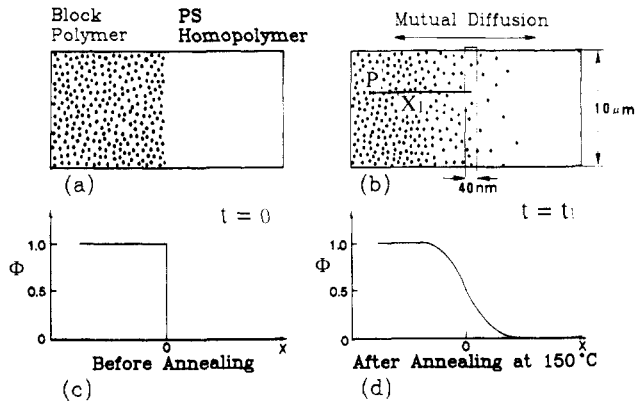

Figure 3. Schematic diagrams on the cross sections of the welded interfaces of the SI diblock polymer and homopolystyrene, (a) before annealing ($t = 0$) and (b) after annealing ($t = t_1$) at 150 °C. The black dots in the figures indicate the spatial distribution of the PI spherical microdomains. The corresponding concentration profiles of the SI diblock polymer across the welded interfaces are shown in c and d, respectively. The concentration profiles were experimentally obtained by counting the number of PI spherical microdomains in the rectangular area of 40 nm by ca. 10 μm on the electron micrographs.

Figure 3. The time-dependent spatial distribution of the centers of mass of the spheres across the interface $\phi(x,t)$ can be experimentally determined by transmission electron microscopy (TEM) as sketched in parts c and d of Figure 3. In this way we can visualize the mutual diffusion process using the microdomains as a probe.

Table I
Characterization of Samples

sample code	sample	M_n[c]	M_w/M_n[d]	PS,[e] wt %
SI[a]	B2	1.7×10^5	1.26	85
HS[b]	TS21	1.0×10^4	1.02	100
HS[b]	H6	6.0×10^4	1.03	100

[a] Poly(styrene-*b*-isoprene). [b] Homopolystyrene. [c] Determined by membrane osmometry. [d] Determined by size-exclusion chromatography. [e] Determined by elemental analysis.

In this paper we present our study on the molecular mechanism of the mutual diffusion process for such systems as described above. The diffusion is proposed to be controlled by a free energy barrier, $\delta\Delta F^*$, associated with a loss of conformational entropy encountered for both PS and HS when HS diffuses into the microdomain space and breaks up the molecular interactions between PS coronas.

II. Experimental Methods

1. Samples. Samples used in this work are characterized in Table I. SI was prepared by living anionic polymerization in tetrahydrofuran (THF) with *s*-butyllithium as the initiator. The homopolystyrene samples were kindly supplied by TOSOH Co., Ltd., Japan.

2. Film Preparations. Film specimens of ca. 0.5-mm thickness were prepared by casting 5.0 wt % toluene solution in Petri dishes. The solvent was slowly evaporated over 14 days at 30 °C. The film specimens thus prepared were further dried in a vacuum oven at 100 °C until a constant weight was attained.

3. Welding Methods and Sample Preparation for Transmission Electron Microscopy. The welding surfaces for both HS and SI specimens were newly prepared immediately before the experiments as follows. The cast films were notched at the surface and fractured at room temperature, and the fresh fracture surfaces were used for welding. The film specimen of HS was first melted on a glass plate placed on a hot plate controlled at 150 °C, which is well above the glass transition temperature of HS. The fracture surface of the block polymer specimen was then welded onto the fracture surface of HS for about 10 s. Then the welded specimen together with the glass plate was quenched into iced water. An attention was paid to minimize the direct contact of the block polymer specimen with the hot glass plate. The welding procedure and the typical shape of the sample specimen after the welding are sketched in parts a and b of Figure 4, respectively.

The rest of the experimental procedure is also sketched in Figure 5. The welded samples were annealed in a vacuum oven at 150 °C for a given period of time t and quenched into iced water. Samples annealed at 150 °C for different time intervals were prepared (Figure 5a). The annealed samples were trimmed and stained for 2–7 days by exposing them to osmium tetroxide vapor. The stained samples were then subjected to ultramicrotoming into ultrathin sections of 50–90-nm thickness in such a way as shown in parts b and c of Figure 5, the knife plane being set normal to both the free surface and welded interface of the specimens. Special care was taken so that the plane of the knife was set parallel to the sample plane, which is normal to the welded interfaces as exactly as possible because it directly affects the reliability of the evaluation of the mutual diffusivity. The welded interfaces of the specimens stained by osmium tetroxide can be clearly distinguished to the eyes under a magnifier, which makes the setting of the knife easier. The thin section contains the pure microdomain phase and pure HS phase across the welded interface as shown in Figure 5c. The ultrathin section was further subjected to the staining by osmium tetroxide vapor on a microscope grid before the transmission electron microscopic (TEM) investigation.

4. Analyses of Spatial Distribution of PI Spheres $\phi(x,t)$ across the Welded Interface. We determined the directions parallel and perpendicular to the welded interface by observing the TEM micrographs containing the interface over a sufficiently large length, at least about 10 μm. We then counted

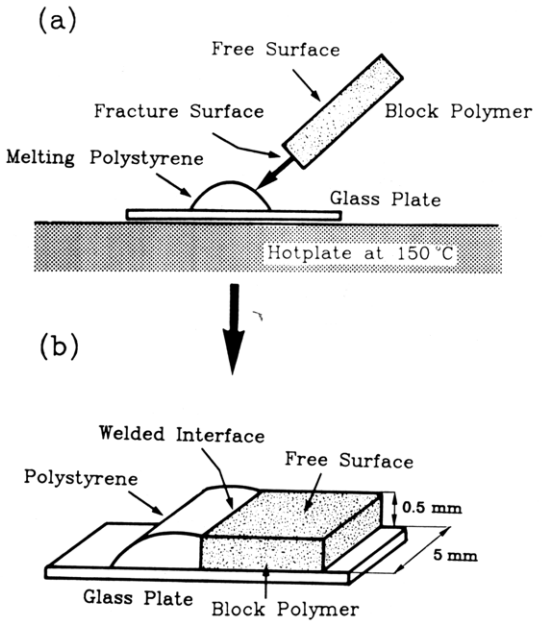

Figure 4. Schematic representations of the preparation technique of the welded specimens. (a) Immediately after a newly created fracture surface of the block polymer film was welded on the molten homopolystyrene placed on a glass plate at 150 °C, the specimen together with the glass plate was quenched into ice water. (b) A view of the welded specimen used in the subsequent annealing experiment.

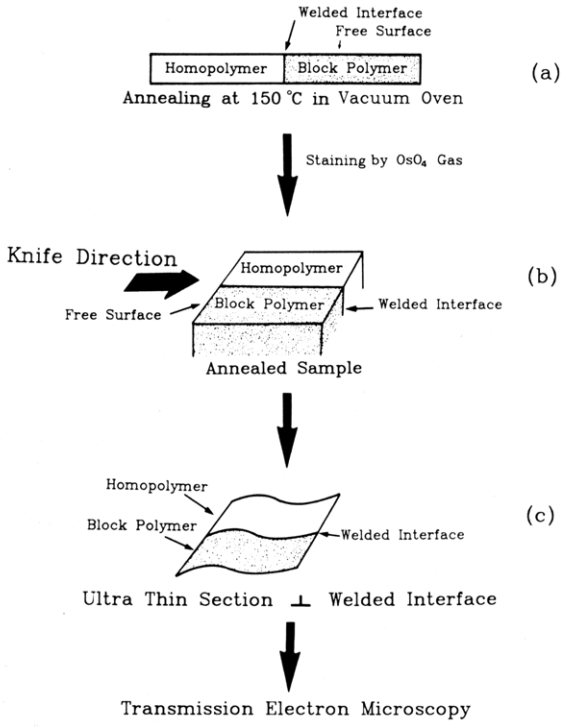

Figure 5. Experimental procedure on electron microscopy of the welded interfaces: (a) a side view of the welded specimen; (b) ultramicrotoming with the plane of knife perpendicular to the film surface and welded interface; (c) an ultrathin section containing the cross section of the welded interface.

the number of dark PI spherical microdomains $N(x_1)$ whose centers were located in the area of a 40-nm width centered at position x_1 from an arbitrarily chosen reference point P along the direction perpendicular to the interface (see Figure 3b). When we determined $\phi(x,t)$, we excluded the positions of the specimens close to the air–polymer interface and the air–glass interface in order to investigate the mutual diffusion in bulk. The area where $N(x_1)$ reaches a constant and maximum value N_{max} corresponds to the place where no HS diffuses in across the

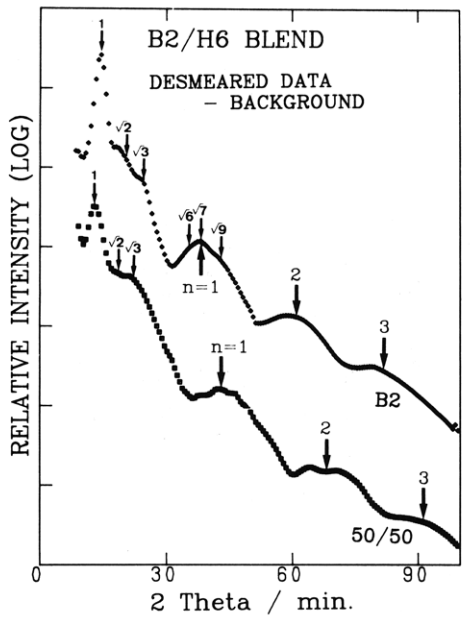

Figure 6. Small-angle X-ray scattering profiles of the SI diblock polymer (B2) and a 50/50 wt % mixture of the SI diblock polymer (B2) and homopolystyrene (H6) corrected for absorption, slit smearing effects, background scatterings, etc.

interface, and the place where $N(x_1)$ becomes zero corresponds to pure HS phase. In order to obtain $\phi(x_1,t)$, the spatial distribution of the centers of PI spheres at time t, we normalized $N(x_1,t)$ by N_{max} when pure SI block polymer was welded with HS

$$\phi(x_1,t) = N(x_1,t)/N_{max} \quad \text{(II-1)}$$

This $\phi(x_1,t)$ changes from 1 to 0 with increasing x_1.

When it is possible, we try to fit $\phi(x_1,t)$ with the error function based on the assumption of one-dimensional Fickian diffusion

$$\phi(x,t) = 0.5\{1 - \text{erf}\,[x/2(Dt)^{1/2}]\} \quad \text{(II-2)}$$

In this case we set the location of the interface at $x = 0$ by choosing the interface by trial and error and by finding the best fit between the experimental and theoretical $\phi(x,t)$'s.

5. Small-Angle X-ray Scattering. Small-angle X-ray scattering (SAXS) profiles of the spherical microdomain systems were measured with a rotating anode X-ray generator of 12 kW with monochromatized Cu Kα line and a 1.5-m X-ray camera with a one-dimensional position-sensitive proportional counter.[5] The profiles were corrected for absorption, background scattering arising from the thermal diffuse scattering, and slit-width and silt-height smearing effects.[6]

III. Experimental Results

1. Microdomain Structure. The microdomain structure for the as-cast films of pure SI block polymer (B2) films and that for a mixture of B2 and H6 with a composition of 50/50 wt % were characterized by SAXS. The SAXS profiles are shown in Figure 6. A number of scattering maxima or shoulders are observed at the positions corresponding to $1:\sqrt{2}:\sqrt{3}:\sqrt{4}$:..., etc., relative to the first-order peak, as shown by the thin arrows, indicating that the spherical microdomains are in a simple cubic (SC) or body-centered cubic (BCC) lattice. The TEM investigation on the stained and ultrathin-sectioned specimens revealed that the spheres comprise PI chains. The nearest-neighbor intersphere distance, D_{sp}, is determined from the Bragg spacing, d_{hkl}, measured from the positions of the scattering maxima, $2\theta_{hkl}$, due to the intersphere interference

$$2d_{hkl} \sin \theta_{hkl} = \lambda \quad \text{(III-1)}$$

Table II
Characterization of Microdomain Structures by SAXS Analyses

sample	R,[a] nm	a,[b] nm	N_b[c]	Ψ_{PI}[d] (SC)	Ψ_{PI}[e] (BCC)	$\Psi_{PI,vol}$[f]
B2	12.9	44.2	194	0.0678	0.1356	0.169
B2:H6 = 1:1	11.2	51.2	127	0.0284	0.0567	0.086

[a] Average radius of the PI spherical microdomain determined by SAXS using eq III-5. [b] Average nearest-neighbor intersphere distance determined by SAXS using eq III-4. [c] Average number of block chains emanating from a single spherical microdomain. [d] Volume fraction of the PI spherical microdomains calculated for an SC lattice with the SAXS data (eq III-6, $k = 1$) where a was calculated using eq III-3. [e] Volume fraction of the PI spherical microdomains calculated for a BCC lattice with the SAXS data (eq III-6, $k = 2$) where a was calculated using eq III-4. [f] Stoichiometric volume fraction of the PI component, with the densities of PS and PI being 1.053 and 0.913 g/cm^3, respectively.

where

$$d_{hkl} = a/(h^2 + k^2 + l^2)^{1/2} \quad \text{(III-2)}$$

λ is the wavelength of X-ray, a is the cell edge of the cubic lattice, and h, k, and l are the Miller indices of the diffraction planes. It should be noted that there are extinction rules in applying eqs III-1 and III-2. D_{sp}, d_{hkl}, and a are interrelated to one another

$$d_{100} = a_{SC} = D_{sp} \quad \text{(III-3)}$$

for SC where a_{SC} is the cell edge for SC, and

$$d_{110} = a_{BCC}/(2)^{1/2} = (2/3)^{1/2}D_{sp} \quad \text{(III-4)}$$

for BCC where a_{BCC} is the cell edge for BCC.

The SAXS profiles show also broad maxima at $2\theta_{max,n}$ due to the intraparticle interference of single spheres as shown by the thick arrows with $n = 1$–3 in Figure 6

$$(4\pi R/\lambda) \sin \theta_{max,n} = 5.765, 9.10, 12.3, \ldots \quad \text{(III-5)}$$

$$\text{for } n = 1, 2, 3, \ldots$$

From the peak positions $2\theta_{max,n}$ one can determine the average radius of the spheres R.[7,8] Thus, from the SAXS profiles we determined R, D_{sp}, the average number of the block chains per single spherical microdomain N_b and the volume fraction of PI spheres, $\Psi_{PI,calc}$, calculated for SC and BCC lattices according to the method as discussed previously[9]

$$\Psi_{PI} = (4\pi/3)k(R/a)^3 \quad \text{(III-6)}$$

where $k = 1$, 2, and 4 for SC, BCC, and FCC (face-centered cubic lattice), respectively, and

$$(4\pi/3)R^3 = N_b\nu_{PI} \quad \text{(III-7)}$$

where ν_{PI} is the volume occupied by a single PI block chain

$$\nu_{PI} = M_{PI}/(\rho_{PI}A) \quad \text{(III-8)}$$

M_{PI} is the molecular weight of PI block chain, ρ_{PI} is the mass density of pure PI (0.913 g/cm^3), and A is Avogadro's number. The estimations of N_b and Ψ_{PI} are based upon the assumptions that PS and PI undergo a complete segregation and that HS is selectively and completely solubilized into the PS matrix. The results were summarized in Table II where Ψ_{PI} was compared with the stoichiometric volume of PI ($\Psi_{PI,vol}$). Comparison of $\Psi_{PI,vol}$ and Ψ_{PI} clearly indicates that the spheres are packed in BCC lattices. It should also be noted that the swelling of the PS matrix phase with HS expands the intersphere distance, causing expansions of a and D_{sp}. The swelling increases also the average nearest-neighbor distance between the chemical junctions of the block polymer chains along the interface, which in turn decreases N_b and hence R (see eq III-7).[10] If HS chains do not mix with PS coronas and HS is segregated out from PS coronas into the regions between the coronas, N_b does not change with HS fraction, and hence R is not affected by the HS fraction. Thus the decrease of R with the HS fraction is due to the swelling of the PS corona by HS. The degree of swelling, in turn, depends on the molecular weight of HS (M_{HS}) relative to that of PS (M_{PS}) for a given block copolymer with a given fraction of PS,[11] the larger the value M_{HS} relative to M_{PS}, the smaller the degree of swelling of the PS corona by HS.

2. TEM Studies on the Mutual Diffusion. TEM investigations were pursued on the welded samples annealed at 150 °C for various time intervals and then followed by staining with osmium tetroxide and ultrathin sectioning. The typical micrographs are shown in Figures 7–10 where the dark spheres correspond to PI spheres selectively stained by osmium tetroxide. Here it should be noted that all the homopolystyrenes used for the welding experiments have M_n values much smaller than that of PS block chains (see Table I).

Figure 7 shows the results for the welded specimens of B2/TS21 where the a–c represent, respectively, the specimen after the welding but before annealing and those 1.08×10^4 and 1.80×10^4 s after the annealing. In each micrograph of Figure 7 and also of Figures 8–10, the upper and lower halves of the picture correspond, respectively, to the pure HS phase (or HS-rich phase) and the initial microdomain phase. The initial microdomain phase is the pure SI phase for the cases of Figure 7–9 and the SI phase containing HS by 50 wt % for the case of Figure 10. The welded interface is flat and sharp before annealing (Figures 7a and 8a), so that the determination of the directions parallel and perpendicular to the interface is not very difficult.

As time elapses after annealing at 150 °C, the interfacial area becomes diffuse normal to the interface, the interfacial thickness being about 2 μm for Figure 7b and 3 μm for Figure 7c at the long time limit covered in our experiment. These micrographs clearly visualize the mutual diffusion of HS into the microdomain space and that of PI spheres with PS coronas into the HS phase. HS chains having M_n lower than that of PS block chains can definitely diffuse into the microdomain space. Thus the mutual diffusion involves a displacement of the interface, as a marker, toward the HS side, i.e., the side having a higher self-diffusivity. This is a phenomenon well-known as the Kirkendall effect[12] in metallurgy. The effect was essentially observed also in the previous reports.[2,13]

Figures 8 and 9 represent typical micrographs for the mutual diffusivity of B2 and HS (H6) having M_n larger than that of TS21. Comparison between the results shown in Figures 7 and 8 shows spectacularly that the mutual diffusion is much slowed down when M_n of HS is increased from 1.0×10^4 (TS21) to 6.0×10^4 g/mol (H6). It should also be noted that the interactions between PI spheres and PS coronas appear to be much stronger against the diffusion of higher molecular weight HS (H6) than that of lower molecular weight HS (TS21), as the spatial distribution of PI spheres near the interfaces for the B2/H6 system is not seen to be quite as random as that for the B2/TS21 system. This is an important observation since it implies that higher molecular weight HS has more difficulty in diffusing uniformly into the matrix of the microdomain and being uniformly solubilized in the space than

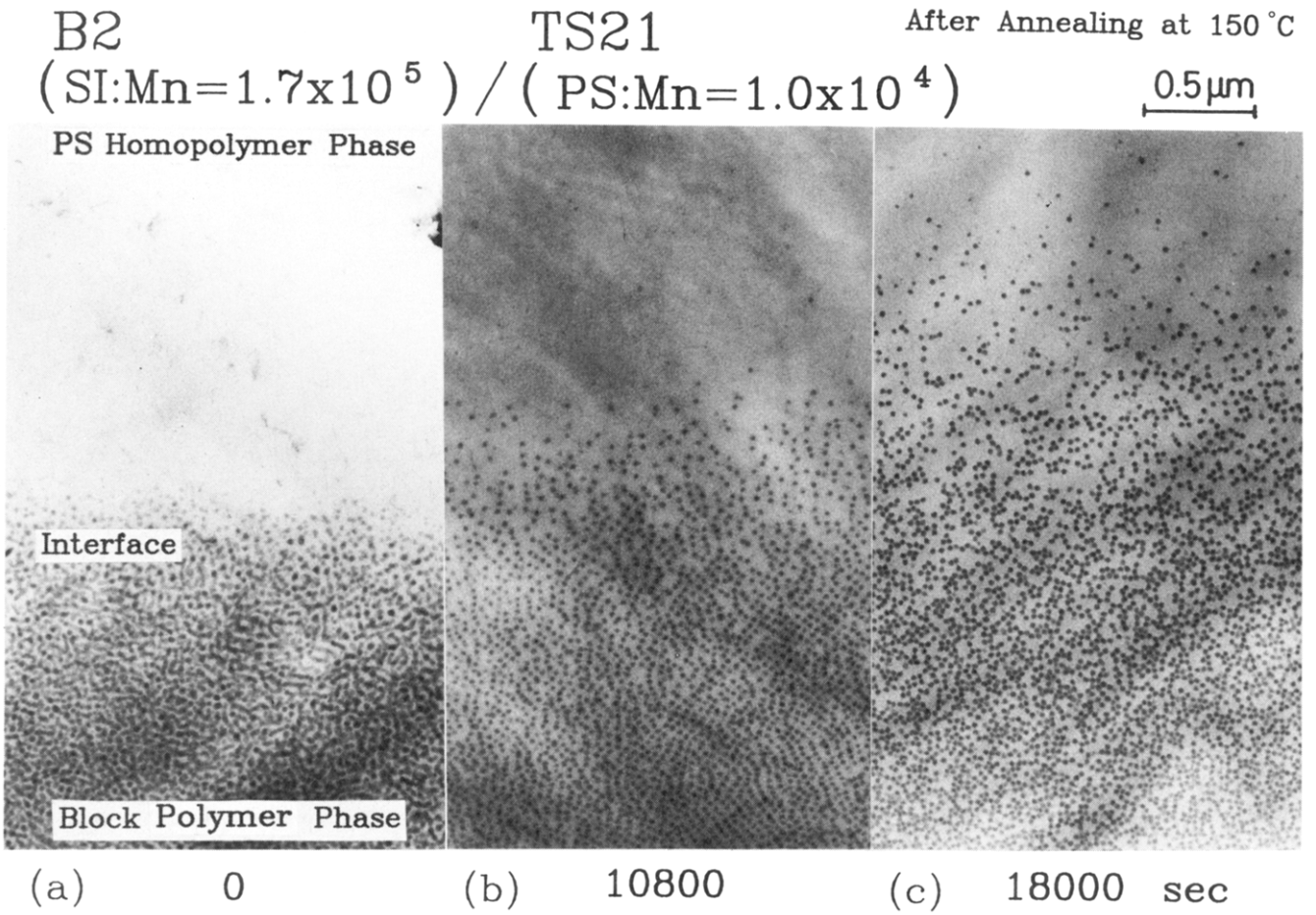

Figure 7. Electron micrographs of the cross sections of the welded interfaces of the SI block polymer (B2) and homopolystyrene (TS21) after annealing at 150 °C for 0, 10 800, and 18 000 s.

lower molecular weight HS. The difference in the interactions between PI spheres against the diffusion of HS having different molecular weight is also manifested in the difference of diffusion mechanism of PI spheres with PS coronas. The mutual diffusion generally involves two modes of diffusion of the spheres: "collective diffusion" and "individual diffusion". The collective (individual) diffusion of the spheres is more prominent in the mutual diffusion with higher (lower) molecular weight HS than with lower (higher) molecular weight HS.

Moreover, the strong interaction between PI spheres against diffusing HS can be highlighted in Figure 9 where it is implied that the diffusion of the spheres in region A far from the welded interface is much faster than the diffusion in region B near the interface. This phenomenon clearly suggests that once interactions between PI spheres and therefore those between PS coronas are screened out by diffusing-in HS, the spheres can diffuse at faster rate. The spheres that still maintain the interparticle interactions tend to diffuse as a member of diffusing clusters (viz., "collective diffusion"). This implies also the fact that the mutual diffusion of the spheres and HS does not obey the simple Fickian diffusion.

The effect of intersphere interactions on the mutual diffusion of B2 and HS is highlighted also by comparing the results shown in Figures 8 and 10. In the experiment shown in Figure 10 the intersphere interactions were intentionally weakened from the beginning by solubilizing HS (H6) into the PS matrix of the spherical microdomain system of SI (B2) (see the case of Figure 1b). This can be accomplished by preparing the solvent-cast film of the mixture of B2 and H6 with the composition of 50/50 wt % (B2:H6 = 1:1), for example, and welding this specimen against the specimen of pure HS (H6). In fact it is clearly observed that the mutual diffusion in the system of the block polymer containing solubilized HS (Figure 10 for (B2:H6 = 1:1)/H6) is much faster than that in the system of the pure block polymer (Figure 8 for B2/H6). Thus HS solubilized into the microdomain space is expected to weaken the interaction between corona PS chains and to enhance the mutual diffusion. For more quantitative discussions one needs to take into account the difference in the intrinsic diffusivity, D_0, of PI spheres with PS coronas, viz., the effect of PI spheres and PS coronas being smaller for a B2/H6 mixture than for pure B2 on the mutual diffusivity (cf. R and N_b in Table II).

3. Spatial Distribution of PI Spheres across the Interface. According to the method as described in detail in section II.4, we determined the spatial distribution of the centers of spheres, $\phi(x,t)$, across the welded interface as a function of time t spent for the annealing process from the TEM pictures as shown in Figures 7–10. The results are summarized in Figure 11 for B2/TS21 and B2/H6 systems and in Figure 12a for B2 initially containing solubilized HS (H6) by 50 wt %, i.e., for the (B2:H6 = 1:1)/H6 system.

It should be noted, however, at this point that our analyses on $\phi(x,t)$ are based upon the following assumptions: (i) The number of PI spheres and their size are conserved during the diffusion, (ii) the microtoming direction and hence the plane of the ultrathin section is perpendicular to the interface, and (iii) the thickness of the ultrathin section is constant and uniform.

If PI spheres which diffuse in the HS phase up to the region where their number density becomes lower than a critical value (critical micelle concentration) happen

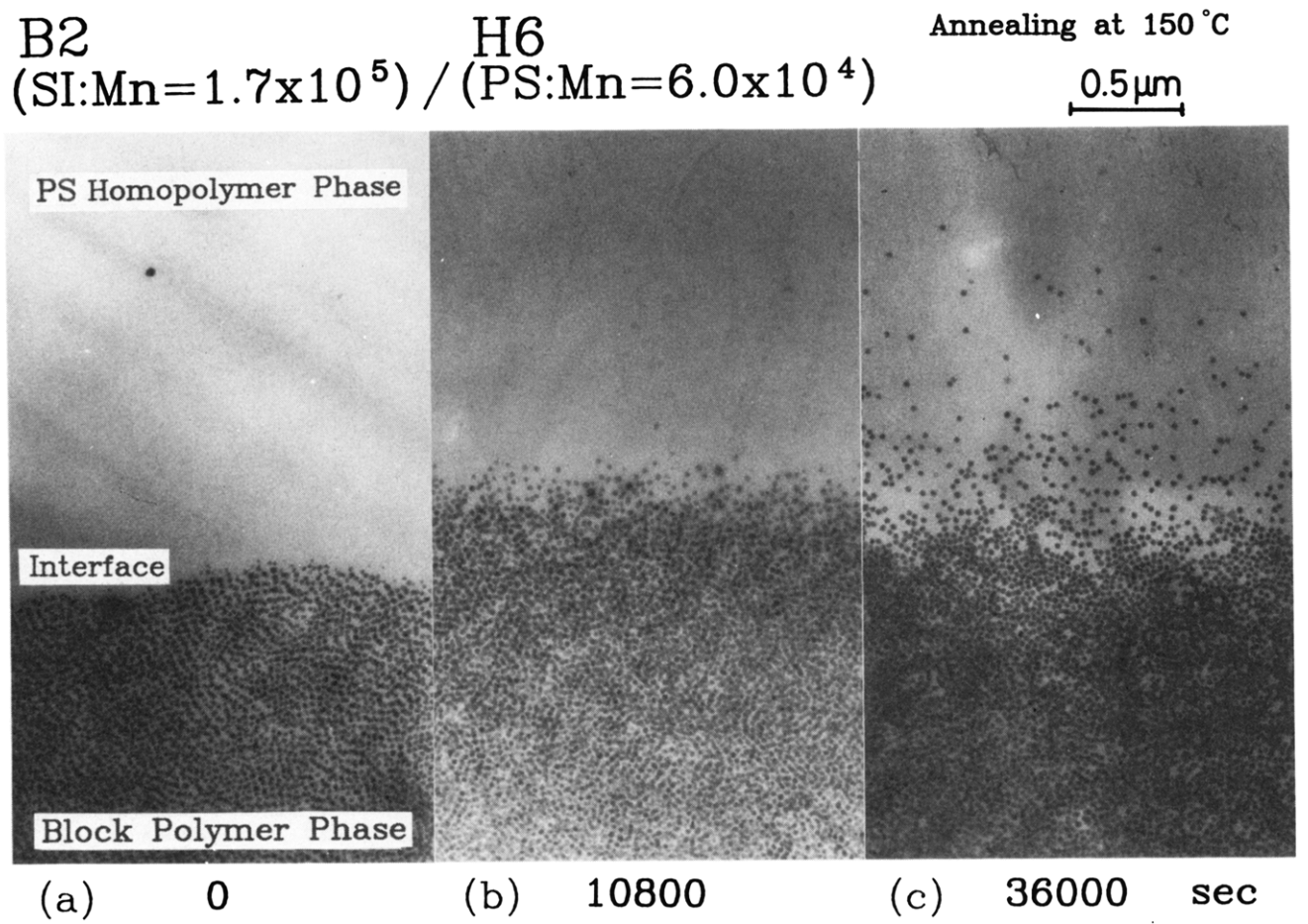

Figure 8. Electron micrographs of the cross sections of the welded interfaces of the SI block polymer (B2) and homopolystyrene (H6) after annealing at 150 °C for 0, 10 800, and 36 000 s.

to be dissolved into the HS phase and annihilate, assumption (i) will not be held. Even in such a case, the profiles we determined are correct, but it alters our interpretation of the profiles. This is simply because in this case we are not seeing the simple mutual diffusion process of HS chains and PI spheres with corona PS chains in the conserved system in terms of the total number of the spheres. The possibility of the annihilation process is itself an interesting research project which might be studied by carefully cross-linking PI spheres only. This deserves future studies. The assumptions (ii) and (iii) are important to ensure accuracy of the measured profiles on $\phi(x,t)$ but strongly depend on the skillfulness of the researchers in the ultramicrotoming technique.

Figure 11 represents comparisons of $\phi(x,t)$'s for the system having low molecular weight HS (i.e., B2/TS21, parts a and b) with those having large molecular weight HS (i.e., B2/H6, parts c–e). The solid lines indicate the results expected for the simple Fickian diffusion (eq II-2) with D = 1.5 nm^2/s for the B2/TS21 system (parts a and b) and with D = 0.5 nm^2/s for the B2/H6 system (parts c–e). It clearly reflects the results of the TEM observations in section III.2; (i) The system with HS having larger molecular weight shows much slower mutual diffusion than that having smaller molecular weight, (ii) the system with HS having smaller molecular weight obeys the simple Fickian diffusion more likely than that having larger molecular weight, and (iii) the deviation from the Fickian diffusion is clearly seen in the regions A and B (shown in parts d and e of Figure 11) for the system with higher molecular weight HS where the regions A and B have, respectively, a higher and a lower diffusion rate than the average diffusivity, 0.5 nm^2/s. This *space-dependent diffusivity* is due to the *space-dependent interactions* between corona PS chains of PI spheres against diffusing-in HS as discussed in section III.2. Due to these interactions between PI spheres, D itself becomes a function of the spatial position x

$$D = D(x; T, M_{HS}, \Psi_{HS}), \qquad \text{(III-9)}$$

as well as a function of temperature T, molecular weight of HS (M_{HS}), and volume fraction of HS in the initial microdomain space (Ψ_{HS}) when HS is mixed with SI from the beginning.

Figure 12 highlights the effect of solubilized HS initially incorporated to the microdomain space where part a corresponds to the result having 50 wt % HS in the B2 phase and part b to that having no HS in the B2 phase. Again the solid lines represent the fits with the simple Fickian diffusion process given by eq II-2 with D = 5 nm^2/s for part a and 0.5 nm^2/s for part b. Thus the data clearly show that solubilized HS enhances the mutual diffusivity. Figure 12a clearly shows the deviation from the simple Fickian diffusion more clearly than Figure 12b. This is primarily because Figure 12a corresponds to the profile at an effectively much later time than Figure 12b. If the time scale of the observation is adjusted such that Dt becomes identical for the two systems, the deviation from the Fickian diffusion is expected to be larger for the B2/H6 system than for the (B2:H6=1:1)/H6 system, because of the stronger interactions between PI spheres for the former.

All the results shown in Figures 11 and 12 imply that the mutual diffusion is non-Fickian. Thus the values D extracted by using eq II-2 should be regarded only as a

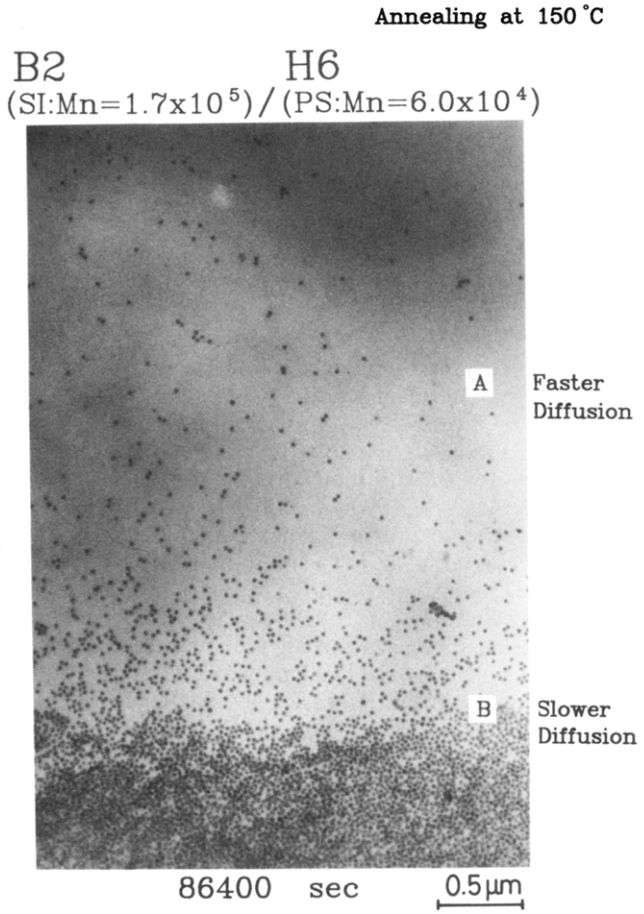

Figure 9. Electron micrograph of the cross section of the welded interface of the SI block polymer (B2) and homopolystyrene (H6) after annealing at 150 °C for 86 400 s. Diffusion of the PI spherical microdomains in region A is much faster than that in region B.

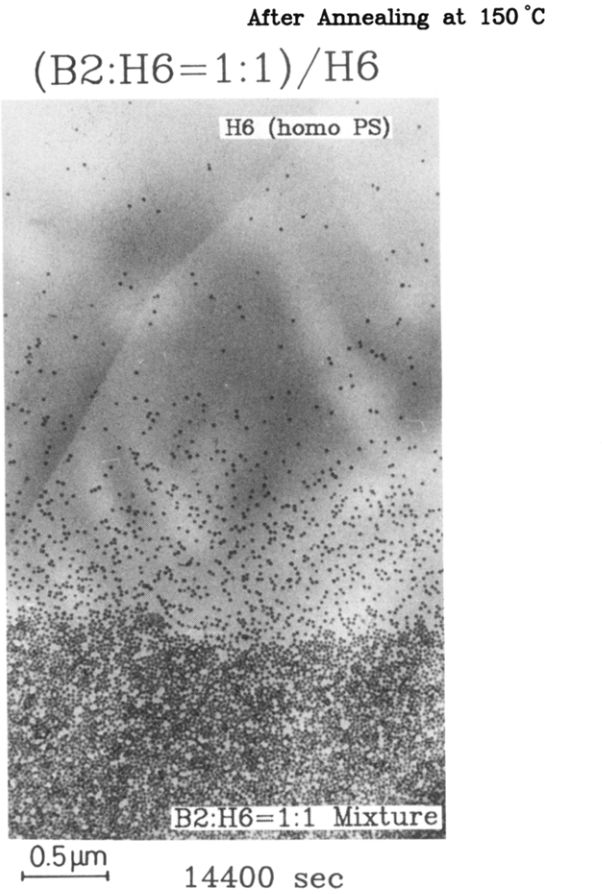

Figure 10. Electron micrograph of the cross section of the welded interface of homopolystyrene (H6) and a 50/50 wt % mixture of SI block polymer (B2) and H6 after annealing at 150 °C for 14 400 s.

very rough measure of D's. D is strongly space- and, hence, concentration-dependent due to the space-dependent interactions between corona PS chains against diffusing-in HS. The analysis of non-Fickian behavior is, however, beyond the scope of the present paper and will be presented in a subsequent paper.

IV. Interpretation and Discussion

Let us now describe our *qualitative* interpretations on the experimental results discussed in section III. Figure 13 shows the sketch of our interpretation, which shows schematically the free energy barrier for the process of the mutual diffusion, leading to the transformation of the structure from the initial state 1 to the final state 2. The initial state is the state after the welding but before the annealing, and the final state is the state where HS molecules are diffused in the microdomain space and distributed, more or less, uniformly in the matrix.

For our study we set the final state **2** as the state where the concentration of PI spheres, ϕ_{sphere}, is lowered in comparison with that for the pure SI phase but is still sufficiently high so that the average concentration of the block polymer, ϕ_{block}, is higher than the critical micelle concentration, ϕ_{cmc}. Since $\phi_{block} = \phi_{sphere}/\Psi_{PI,vol}$, $\Psi_{PI,vol}$ being the volume fraction of PI block chains in the SI block polymer, this criterion is rewritten as $\phi_{sphere} > \phi_{cmc}\Psi_{PI,vol}$. Thus we discuss the diffusion process under this criterion where no microdomains are dissolved into the matrix. It should be noted that as time elapses the criterion of $\phi_{sphere} < \phi_{cmc}\Psi_{PI,vol}$ is locally satisfied. In such a region, the microdomains may be eventually dissolved into the matrix by a thermal activation process. The system will eventually attain the equilibrium situation with no microdomains. The dynamical study on such a thermally acti-

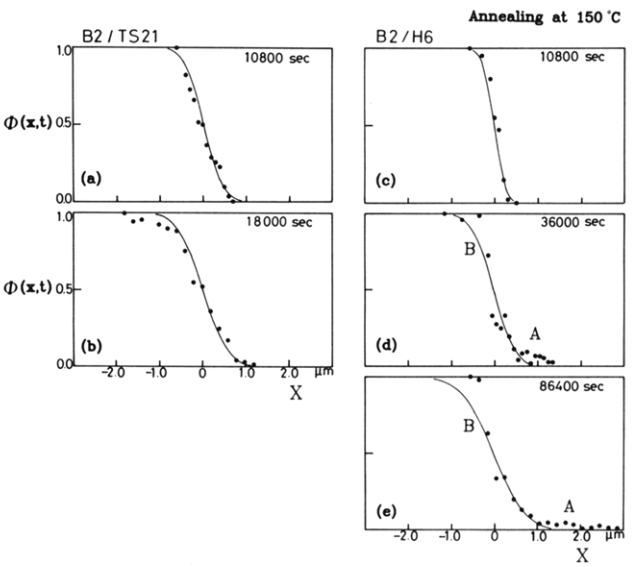

Figure 11. Spatial distribution of PI spherical microdomains $\phi(x,t)$ across the welded interface as a function of annealing time at 150 °C: (a) 10 800 s and (b) 18 000 s for the mutual diffusion between the SI block polymer (B2) and homopolystyrene (TS21); (c) 10 800 s; (d) 36 000 s; and (e) 86 400 s for the mutual diffusion between B2 and homopolystyrene (H6). The solid lines show the best fit of the measured $\phi(x,t)$'s with the simple Fickian diffusion (eq II-2) with D = 1.5 nm²/s for (a) and (b) and 0.5 nm²/s for (c)–(e).

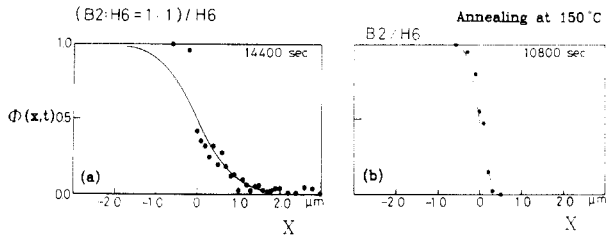

Figure 12. Comparison of the spatial distributions of PI spherical microdomains $\phi(x,t)$ across the welded interfaces between (a) the mutual diffusion between homopolystyrene (H6) and a 50/50 wt % mixture of the SI block polymer (B2) and HS (H6) and (b) the mutual diffusion between H6 and pure SI block polymer (B2). The solid lines show the best fit of the measured $\phi(x,t)$'s with the simple Fickian diffusion (eq II-2) with D = 5 (a) and 0.5 nm²/s (b).

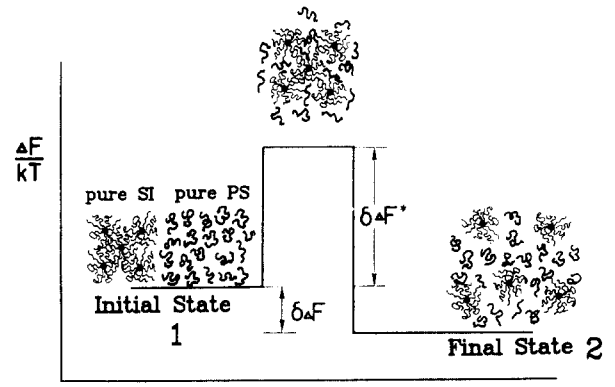

Figure 13. Change of free energy during the process of the mutual diffusion between the SI diblock polymer with PI spherical microdomains and homopolystyrene (HS). There is an energy barrier for the mutual diffusion process that causes the change from the initial state (1) and the final state (2). This barrier is due to the excess free energy, $\delta\Delta F^*$, required for the solubilization of diffusing-in HS into the PS matrix of the microdomains.

vated dissolution process of the microdomains is an interesting research topic but is beyond the scope of this paper.

There will be a small decrease of free energy ($\delta\Delta F$) associated with a small increase of the combinatorial entropy for the change from state 1 to state 2, and this decrease of the free energy becomes the thermodynamic driving force for the mutual diffusion. However, the mutual diffusion has to overcome the free energy barrier, $\delta\Delta F^*$, which is the excess free energy required for the solubilization of HS into the PS matrix of the microdomains during the diffusion process. The solubilization generally involves a loss of conformational entropy of PS block chains and HS chains and hence causes a penalty of the conformational free energy $\delta\Delta F^*$. The mutual diffusion takes place when the thermal energy k_BT overcomes this free energy barrier, $\delta\Delta F^*$, and hence

$$D = D_0 \exp(-\delta\Delta F^*/k_BT) \qquad \text{(IV-1)}$$

D_0 is an intrinsic diffusivity of PI spheres with corona PS chains in the matrix of HS in the case when $\delta\Delta F^* = 0$, i.e., the case where the interactions between corona PS chains are screened out by preexisting HS. Thus D_0 is the D value in the case when corona PS chains attached to PI spheres are sufficiently far apart in the medium of HS. $\delta\Delta F^*$ depends on the interaction between corona PS chains and hence on the local concentration of HS, which in turn results in space-dependent $\delta\Delta F^*(x)$ and $D(x)$.

The free energy barrier, $\delta\Delta F^*$, was found to be a function of M_{HS}, and Ψ_{HS}, the volume fraction of HS solubilized initially in the block polymer microdomain space for a given block polymer SI

$$\delta\Delta F^* = f(M_{HS},\Psi_{HS}) \quad \text{for given SI} \qquad \text{(IV-2)}$$

It was found that the smaller the value of M_{HS} and the larger the value of Ψ_{HS}, the smaller the value of $\delta\Delta F^*$ and hence the larger the value of D. During the diffusion process the local concentration profile of HS changes with time, which in turn causes $\delta\Delta F^*$ to depend on space x, resulting in a non-Fickian diffusion.

V. Conclusions

(i) The mutual diffusion process was visualized under TEM observations by using the microdomain structure of a block polymer as a probe.

(ii) Mutual diffusivity D of homopolystyrene (HS) and PI spherical microdomains with many corona PS block chains depends on the molecular weight of HS (M_{HS}) and the amount of HS (Ψ_{HS}) initially solubilized in SI microdomain space, for a given block polymer SI. The larger the Ψ_{HS} value and the smaller the M_{HS} value, the larger the D value.

(iii) D is primarily controlled by $\delta\Delta F^*$, the free energy barrier for the solubilization of HS in the matrix of the microdomain system of SI block polymer, which is required for the mutual diffusion process. Obviously $\delta\Delta F^*$ is larger for larger M_{HS} and for smaller Ψ_{HS}.

(iv) The volume fraction of HS changes in space and is a function of x, which results in space-dependent $\delta\Delta F^*$ and D. Thus $D = D(x;M_{HS},\Psi_{HS})$, and hence the diffusion is non-Fickian.

Acknowledgment. This work was supported in part by a scientific grant from Asahi Glass Foundation for Industrial Technology, Japan (Special Aided Researches). This work was also supported by a Grant-in-Aid for Scientific Research (63470090) from the Ministry of Education, Science and Culture, Japan.

References and Notes

(1) Klein, J.; Briscoe, B. J. *Proc. R. Soc., London A* **1979**, *365*, 53.
(2) Kramer, E. J.; Green, P. F.; Palmstrom, C. J. *Polymer* **1984**, *25*, 473. Green, P. F.; Palmstrom, C. J.; Mayer, J. W.; Kramer, E. J. *Macromolecules* **1985**, *18*, 501.
(3) Green, P. F.; Doyle, B. L. *Phys. Rev. Lett.* **1986**, *57*, 2407. Green, P. F.; Millis, P. J.; Kramer, E. J. *Polymer* **1986**, *27*, 1063.
(4) Green, P. F.; Russell, T. P.; Jerome, R.; Granville, M. *Macromolecules* **1989**, *22*, 908; **1988**, *21*, 3266.
(5) Hashimoto, T.; Suehiro, S.; Shibayama, M.; Saijo, K.; Kawai, H. *Polym. J.* **1981**, *13*, 501.
(6) Fujimura, M.; Hashimoto, T.; Kawai, H. *Mem. Fac. Eng., Kyoto Univ.* **1981**, *43*, 224.
(7) The estimation of R based on eq 5 assumes the monodispersity in the size distribution R. A rigorous evaluation of R in the case when there is a size distribution involves the best fitting between the theoretical and experimental scattering curves, which was discussed in detail elsewhere.[8]
(8) Hashimoto, T.; Fujimura, M.; Kawai, H. *Macromolecules* **1980**, *13*, 1660.
(9) Shibayama, M.; Hashimoto, T.; Kawai, H. *Macromolecules* **1983**, *16*, 16.
(10) Hashimoto, H.; Fujimura, M.; Hashimoto, T.; Kawai, H. *Macromolecules* **1981**, *14*, 844.
(11) Hashimoto, T.; Tanaka, H.; Hasegawa, H. *Macromolecules*, in press.
(12) Smigelskas, A.; Kirkendall, E. *Trans. Am. Inst. Min., Metall. Pet. Eng.* **1947**, *171*, 130. Lazarus, D. in *Solid State Physics*; Seitz and Turnbull, Eds.; Academic Press: New York, 1960; Vol. 10, p 71.
(13) Jordan, E. A.; Bell, R. C.; Donald, A. M.; Fetters, L. J.; Jones, R. A. L.; Klein, J. *Macromolecules* **1988**, *21*, 235.

Registry No. SI (block copolymer), 105729-79-1; PS, 9003-53-6.